

光学学报

基于飞秒激光自调制的高数值孔径微透镜阵列 制备

苑欣然¹, 邓景扬¹, 徐地华¹, 孙相超², 于颜豪^{2*}, 陈岐岱²

¹广东正业科技股份有限公司, 广东 东莞 523000;

²吉林大学电子科学与工程学院, 吉林 长春 130012

摘要 针对硬质材料高数值孔径(NA)微透镜阵列制备难的问题, 提出一种基于像差的自调制激光加工方法。该方法将飞秒激光聚焦于石英衬底的下表面, 能够实现对激光焦点的纵向拉伸, 结合氢氟酸溶液湿法刻蚀实现了具有高数值孔径微透镜的制备。结果表明, 利用该技术通过改变单脉冲能量能够对微透镜形貌进行调控, 在此基础上进一步优化离焦位置, 有效地增大了微透镜的数值孔径, 制备出达到理论极限($NA_{max}=0.46$)的高数值孔径石英微透镜。相对于传统的正面加工方法, 所提方法方式不仅提升了微透镜的数值孔径, 而且无需复杂的光调制系统, 对于高性能硬质材料微透镜阵列的制备与实际应用具有重要的意义。

关键词 激光技术; 飞秒激光加工; 高数值孔径; 微透镜阵列; 熔融石英

中图分类号 TN249

文献标志码 A

DOI: 10.3788/AOS230896

1 引言

微透镜及其阵列具有小型化、易于集成等优点, 在激光均匀化^[1]、超快成像^[2-3]、人工复眼^[4]、虚拟现实(VR)^[5]、增强现实(AR)^[6]等领域具有广泛的应用。透镜的数值孔径(NA)是影响成像质量的重要参数之一。微透镜的景深与 NA 的平方成反比, 分辨率与 NA 成正比, 因此, 要想获得具有更高分辨率的图像, 就需要光学系统具备更大的 NA , 但相应地会失去一部分景深, 观察范围变小。在微成像领域, 通过在一个平面上制造具有不同 NA 的多个微透镜, 在保证成像质量的前提下能够扩大成像的景深范围^[7]。因此, 高效地制备出具有可控高 NA 的微透镜及其阵列是提升成像效果的关键。

目前, 面向不同应用和材料的微透镜阵列的制备^[8], 已经提出金刚石车削^[9]、光刻^[10]、喷墨打印^[11]等技术, 但这些技术在加工材料、加工精度以及形貌控制等方面仍然存在问题。例如: 光刻技术能够实现高精度微纳结构的制备, 但无法精确控制微透镜的面形; 金刚石单点切削虽然可以加工复杂的光学面形, 但加工材料通常仅限于聚合物和有色金属, 而且加工时对金刚石刀具的磨损也非常严重^[12]; 喷墨打印法和纳米压印法主要用于聚合物等软质材料结构的制备, 无法用于

石英、蓝宝石等硬脆材料^[13]。

飞秒激光具有窄脉冲宽度和高瞬时能量的特点, 在硬脆材料三维微纳结构加工方面具有着独特的优势, 目前已经有多项研究利用湿法刻蚀辅助激光加工技术实现了多种硬质材料微透镜及不同形状微透镜阵列的制备^[14-16]。在石英玻璃上制造平面微透镜阵列时最常见的做法是利用飞秒激光对材料正面进行改性, 然后通过化学腐蚀液实现选择性去除并形成微透镜^[17]。但是, 在加工过程中材料表面受到损伤, 导致激光能量损耗, 从而无法实现深结构加工, 造成激光改性区域深宽比小, 难以制备高 NA 的微透镜。为了提高激光加工改性区的深宽比, 人们进行了广泛的光场调制研究: Liu 等^[18]利用空间光调制器将高斯光束调制为细长的贝塞尔光束; Qin 等^[19]利用马赫-曾德尔干涉仪实现时间整形激光束, 将高斯光束分成两个延时子脉冲, 利用时间延迟脉冲串来获得理想的改性形状。这些基于光场调制的技术实现了高 NA 的石英微透镜, 其 NA 达到理论极限(0.46), 但这些技术需要依赖于精确的光场调制, 工艺复杂。为此, 本文提出一种基于像差的自调制激光加工技术, 将激光光斑聚焦在材料下表面后, 由于介质折射率失配和自聚焦效应, 激光光斑在纵向产生了拉伸现象, 无需多次扫描即可实现高深宽比改性结构的制备。结合湿法刻蚀, 成功得到

收稿日期: 2023-05-04; 修回日期: 2023-06-02; 录用日期: 2023-06-07; 网络首发日期: 2023-07-12

基金项目: 广东省基础与应用基础研究基金(2019B1515120081)

通信作者: *yanhao_yu@jlu.edu.cn

NA可调的微透镜阵列，并且达到石英微透镜的NA理论极限。

2 基本原理

2.1 利用基于像差的激光自调制法制备具有高深宽比改性区域的原理

当进行常规的正面加工时，激光光斑的直径 d_0 为平面波聚焦时第一艾里斑直径，纵向长度 L_0 为二倍的瑞利长度^[20]，则有

$$d_0 = \frac{1.22\lambda}{NA_0}, \quad (1)$$

$$L_0 = \frac{n\pi d_0^2}{2\lambda}, \quad (2)$$

式中： λ 为入射激光的波长； NA_0 为物镜的数值孔径； n 为空气折射率。实验中使用放大40倍、数值孔径为0.75的干物镜，计算出在空气中聚焦的光斑直径和纵向长度分别为1.68 μm和4.28 μm。

当飞秒激光通过物镜聚焦后在材料内部进行加工时，紧密聚焦的激光通过两种不同材料的界面传播，折射率的失配会产生纵向的球面像差，导致激光聚焦光斑纵向尺寸增大，这种球差现象随着物镜数值孔径的增大以及聚焦深度的增加而变得愈发明显。已经有许多研究者对于光斑拉长的现象进行了观察、计算和仿真^[20-23]。由球差导致的激光光斑几何形状变化如图1所示，其中 f_0 为空气中的几何焦点， f_d 为近轴焦点位置（聚焦深度）， d_{LA} 为由纵向球面像差引起的焦点拉长距离。相关尺寸数值可以由以下公式^[20]计算得到

$$f_d = n_{\text{silica}} \cdot f_0, \quad (3)$$

$$d_{LA} = \frac{f_d}{n_{\text{silica}}} \left(\sqrt{\frac{n_{\text{silica}}^2 - NA_0^2}{1 - NA_0^2}} - n_{\text{silica}} \right), \quad (4)$$

式中： n_{silica} 为石英玻璃的折射率，取1.46。

由式(4)可以计算出激光聚焦在500 μm厚的石英衬底下表面处的光斑理论总长度为149 μm。激光聚焦光斑的能量分布一般由点扩展函数强度(3-D IPSF)进行计算，随着激光聚焦深度的增加，激光光斑会逐渐出现多个能量高峰，并且峰值能量逐渐减小^[23]，因此在实际加工中，可以对石英衬底进行改性的光斑长度小于理论值，但同时明显大于光斑聚焦在材料上表面时的纵向长度4.28 μm。

形成具有高深宽比的改性区域不仅仅是因为球差。飞秒激光聚焦光斑处的能量密度很高，在经过物镜聚焦后能量密度可以高达 $10^{14}\sim 10^{15} \text{ W/cm}^2$ 。被这样高强度的激光作用的介质材料中会出现非线性效应，其折射率大小会随着光强而变化。在实际的加工过程中，激光能量呈现出高斯分布，被激光照射的介质材料的横向折射率也呈现出相应的高斯分布，这种非线性效应就如同一个会聚透镜将光斑聚焦于材料的内部^[24]。当激光的能量逐渐增大时，这种自聚焦效应更

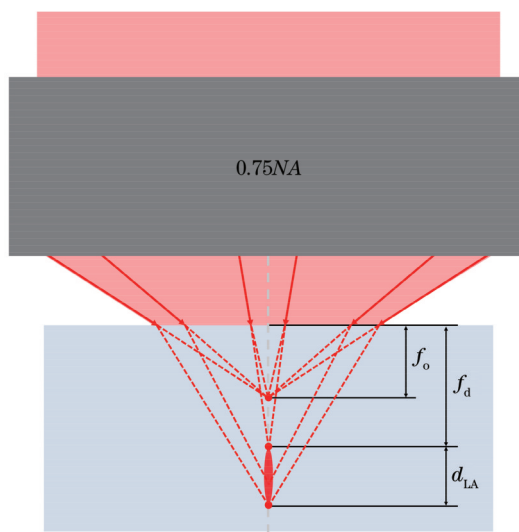


图1 激光从空气进入衬底时由球差现象引起的光斑几何形状改变

Fig. 1 Change of spot geometry caused by spherical aberration when laser focusing across a plane interface from air into the sample

加强烈，光斑会沿着激光传播的反方向有一定的拉长^[20]，这进一步增加了光斑的纵向长度。此外，当高强度飞秒激光作用到透明材料时，表面处于平衡态的电子通过雪崩电离、隧穿效应、多光子电离等非线性过程从价带跃迁到导带成为自由电子，进一步形成高密度等离子体，对衬底材料产生损伤和改性。当多个激光脉冲作用在材料的上表面时，前面的脉冲在表面上产生的损伤区域会阻碍之后的脉冲能量与材料表面的相互耦合；当激光聚焦于衬底材料的下表面时，因为激光从材料的上方入射，所以在材料下表面产生的损伤区域反而增强了材料对激光能量的吸收，促进了高深宽比改性区域的形成。

需要注意的是，这种基于球差的聚焦光斑拉长现象受到物镜数值孔径、衬底材料折射率以及聚焦深度的强烈影响，所以将本文方法应用于具有不同折射率和厚度的材料时，需要重新对光斑的纵向尺寸进行计算，确认其是否满足应用需求。

实验加工光路如图2所示，实验中使用的高重复频率固体飞秒激光器来自Light Conversion公司，脉冲宽度约为300 fs，中心波长为1030 nm，脉冲重复频率为1 MHz，输出光的类型为线偏振光。飞秒激光经过一个扩束器(GCO-2502)扩束至直径为1 cm以覆盖物镜的入瞳，物镜固定在Z方向的单轴气浮平台上，可以通过程序控制其在Z方向的移动。样品放在二维气浮平台(Aerotech-ABL500)上，通过程序控制二维平台在X方向和Y方向移动，气浮平台的分辨率为5 nm，重复定位精度为50 nm。在利用基于像差的激光自调制法制备单个微透镜的过程中，激光的离焦位置是固定的，不需要沿激光传播方向移动衬底或物镜，只需在

确定的位置进行激光加工,即可对高深宽比激光改性区域进行相应的调控。使用反射式激光共聚焦显微镜

(LEXT OLS4100)测量不同微透镜的直径与深度。

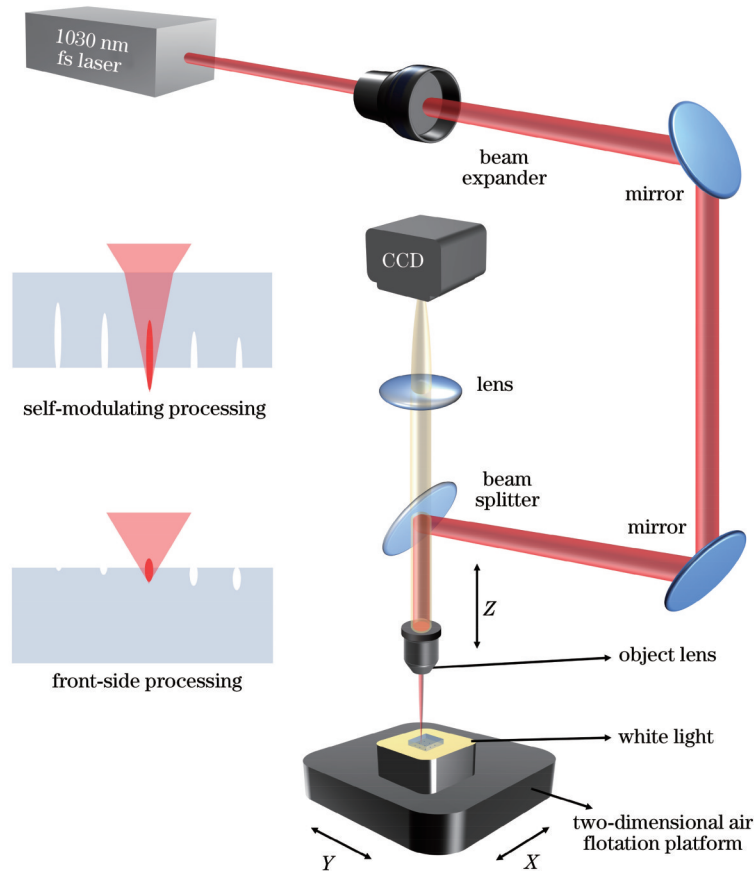


图2 自调制飞秒激光加工系统光路图

Fig. 2 Lightpath of self-modulating femtosecond laser processing system

2.2 湿法刻蚀微透镜原理

氢氟酸(HF)溶液刻蚀激光改性区石英的速率远高于刻蚀未改性区域的速率,这是因为改性区域形成了以平面三元环结构为代表的应变Si—O—Si键,它比稳定的六元环结构更容易受到HF攻击^[25]。因此,微透镜的湿法刻蚀可大致分为两个阶段^[18]:第一阶段是激光改性区域与HF溶液的快速各向异性反应,在这个阶段,激光改性区域被完全腐蚀;第二阶段是未改性的石英本体与HF溶液的各向同性反应。改性区域的深宽比对刻蚀后微透镜的形貌起决定性作用,并进一步影响NA的大小。如图3(a)所示,改性区域纵向深度影响着微透镜深度,而微透镜最终宽度可以由刻蚀时间调控。

本实验使用高纯度JGS1石英,厚度为500 μm,购自无锡市晶禾光学仪器有限公司。综合考虑刻蚀选择性和微透镜形貌两个要求,选择质量分数为20%的HF溶液在25 °C的环境下刻蚀微透镜。刻蚀后,用去离子水冲洗并超声样品10 min,确保无HF残留,样品表面清洁。

设置重复频率为1 kHz,激光单脉冲能量为

238 nJ,制造单个微透镜所需的脉冲数固定为200,分别利用常规正面加工和所提出的自调制法对石英衬底进行激光加工,并用质量分数为20%的HF在25 °C下进行湿法刻蚀。图3(b)、(c)分别展示了常规正面加工和自调制加工在湿法刻蚀0、20、70 min所得结构的共聚焦三维图像,其中图3(b1)、(c1)所示的微小损伤对应于图3(a)的激光烧蚀区域,图3(b2)、(c2)对应于图3(a)中光改性区域被完全刻蚀,此时结构显示出光改性区域的大致形状,图3(b3)、(c3)则展示了最终形成的微透镜形貌。可以看到,在两种加工方法加工出的微透镜直径差距较小的情况下,利用常规正面加工方法加工的微透镜的深度明显小于用自调制法制备的微透镜。

3 实验过程及结果分析

3.1 高数值孔径微透镜的加工

探究由不同脉冲能量加工出的微透镜的形貌特征变化。设置激光器的重复频率为1 kHz,加工单个微透镜的脉冲数固定为200,激光单脉冲能量从157 nJ增加至309 nJ。加工时在激光单脉冲能量为157 nJ的

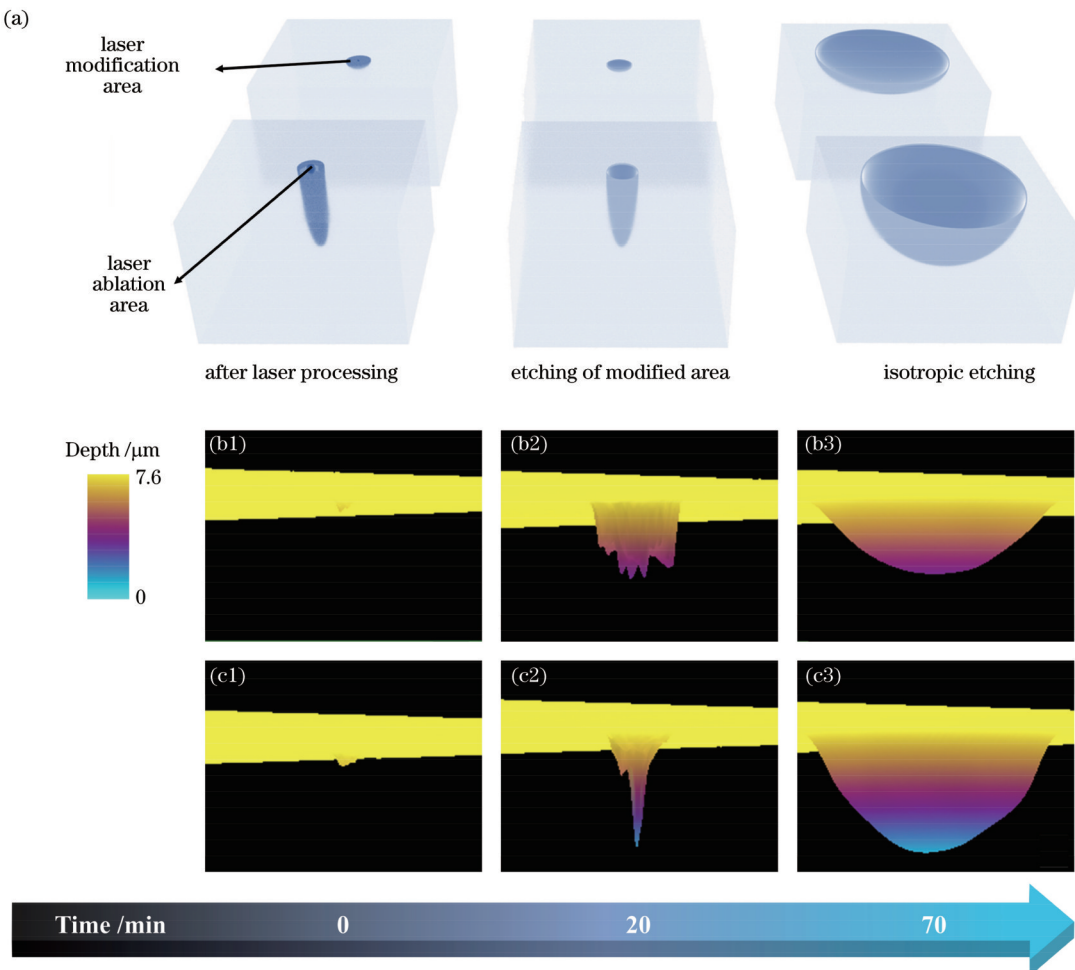


图3 湿法刻蚀形成微透镜结构的过程对比。(a)正面加工和自调制加工方法制备微透镜时刻蚀过程的对比示意图;(b)常规正面加工方法在湿法刻蚀0、20、70 min后所得结构的共聚焦三维图像;(c)自调制法在湿法刻蚀0、20、70 min后所得结构的共聚焦三维图像

Fig. 3 Comparison of the process of forming microlens by wet etching. (a) Comparison of etching process between front-side processing method and self-modulating processing method; (b) confocal 3D images of the structure with regular front-side processing method when etching 0 min, 20 min, and 70 min; (c) confocal 3D images of the structure with self-modulating method when etching 0 min, 20 min, and 70 min

情况下将激光光斑聚焦在石英衬底的下表面,调整光斑的聚焦位置以保证下表面可以产生损伤,加工完单个微透镜后沿横向移动足够远的距离以保证湿法刻蚀后微透镜的完整性,沿激光传播方向不改变衬底和物镜的位置,调整激光单脉冲能量后进行下一个微透镜的加工。加工完成后用质量分数为20%的HF溶液在25 °C刻蚀90 min,制备出的微透镜形貌如图4所示。从图4(a)、(b)可以看到,微透镜的边缘比较光滑,呈现出均匀的圆形,微透镜的宽度由10.7 μm增加到22.1 μm,深度由1.2 μm增加到6.8 μm。

本研究中制造的微透镜均属于平凹球面透镜,根据其成像原理,可以通过微透镜的深度 h 和半径 r 计算得到微透镜的曲率半径 R 、焦距 f 和数值孔径 NA 。所用的相关公式^[14]为

$$R = \frac{h^2 + r^2}{2h}, \quad (5)$$

$$f = \frac{R}{n_{\text{silica}} - n}, \quad (6)$$

$$NA = \frac{r}{f}。 \quad (7)$$

根据式(5)~(7),当微透镜的深度和半径相等($h=r=R$)时,可以达到 NA 理论最大值0.46。由式(5)~(7)计算出上述微透镜的 R 和 NA ,结果如图4(c)所示。当激光单脉冲能量为157 nJ时,微透镜的曲率半径为12.8 μm;当单脉冲能量增加到196 nJ时,曲率半径减小了1.4 μm。这是因为激光单脉冲能量增大,改性区域的深度增加,相应的曲率半径减小;随着单脉冲能量的继续增加,激光改性区域的深度变化量减小,直径的增加量相对较大,导致对应的微透镜曲率半径增大。微透镜曲率半径的变化量为1.46 μm, NA 的变化范围为0.19~0.41,当单脉冲能量为309 nJ时, NA 达到0.41。

为了充分利用自调制加工时激光光斑呈现出的纵

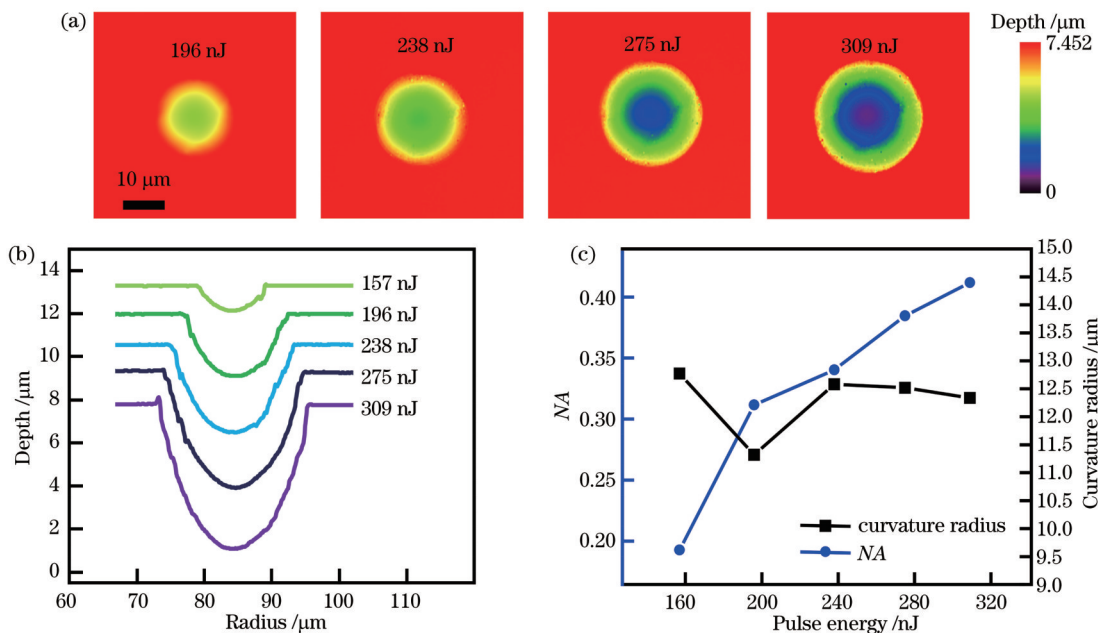


图4 探究在不同的激光单脉冲能量下利用自调制法加工的微透镜的形貌特征。(a)不同脉冲能量下微透镜的共聚焦显微镜等高线图像;(b)不同脉冲能量下制备的微透镜的截面轮廓;(c)微透镜的数值孔径和曲率半径随脉冲能量的变化

Fig. 4 Morphology parameters of microlenses processed by self-modulating method with different pulse energies. (a) Confocal microscope pictures of microlenses at different pulse energies; (b) cross-section profiles of microlenses prepared at different pulse energies; (c) numerical aperture and radius of curvature of the microlens vary with the pulse energy

向较长的椭圆状,在保证表面损伤的前提下,调整光斑位置使其完全聚焦在石英内部,以获得深宽比更大的改性区域。为此,选取的重复频率为1 kHz,加工单个微透镜的脉冲数固定为200,激光单脉冲能量为238 nJ。利用自调制方法加工时,定义刚好能使下表面产生损伤的离焦位置为1 μm,在加工时保证衬底和物镜在激光传播方向固定,每加工完一个微透镜,光斑的位置就向上(向石英内部)移动1 μm,共移动14 μm;在用于对照的正面加工实验中,定义刚好能使上表面产生损伤的离焦位置为1 μm,在加工时同样保证衬底和物镜在激光传播方向固定,每加工完一个微透镜,光斑就向下(向石英内部)移动1 μm。在实验过程中发现,正面加工离焦位置大于等于6 μm时,光斑将完全进入石英内部,此时表面没有损伤,无法刻蚀出微透镜。

利用质量分数为20%的HF溶液在25 °C刻蚀90 min后,微透镜的横截面轮廓如图5(a)所示,可以直观地看到,随着离焦位置的深入,微透镜的宽度和深度都逐渐增加。图5(b)、(d)展示了自调制加工以及正面加工方法制备的微透镜的宽度和深度信息,两种加工方法制备的微透镜的深度和宽度均随着离焦位置的增加近似线性增加。利用自调制法加工出的微透镜宽度略大于正面加工法制备的微透镜,其深度接近于正面加工法制备的微透镜的两倍。如图5(c)、(e)所示,正面加工法制备的微透镜NA最大值仅为0.33,而自调制法加工的微透镜的NA由离焦位置1 μm处的0.30

增加至离焦位置11 μm处的理论极限值0.46后略有减小,这是因为在NA最大时微透镜呈半球形,离焦位置的进一步增加使微透镜的深度大于半径,此时的结构不再属于球面透镜的范畴,可以通过进一步延长刻蚀时间来达到NA最大值。上述结果证明了自调制法在加工高深宽比改性区域方面具有很大优势。

表1所示为相关文献中微透镜的制造方法和相应的NA信息,为了保证对比的准确性及合理性,NA值均由式(5)~(7)计算,其中 n_{silica} 列对应相应文献中在计算NA时所用到的衬底折射率,由于衬底的折射率会随着测试光源的波长而变化,进而影响NA的理论极限值,因此在进行折射率不同的微透镜NA对比时需要格外注意。对比发现:设备较为复杂的脉冲延时调制法以及空间光调制法可以实现石英微透镜NA的理论最大值;一些研究对常规的正面加工方式进行改进,单次曝光后在Z轴方向移动一定的距离,通过多次曝光加工出更长的改性区域,提升了NA的数值,但均未达到其理论最大值。相比之下,所提出的自调制加工技术不仅成功达到了NA的理论极限值,超过了大部分设备复杂的加工方法以及改进的常规加工方法,而且具有设备简单、加工高效等特点。

3.2 微透镜阵列的加工以及成像性能测试

利用激光自调制法在石英衬底的背面加工大规模的微透镜阵列,实验参数设置如下:重复频率为1 kHz,加工单个微透镜的脉冲数为200,激光单脉冲能量为238 nJ,离焦位置选为8 μm,激光加工过程中聚

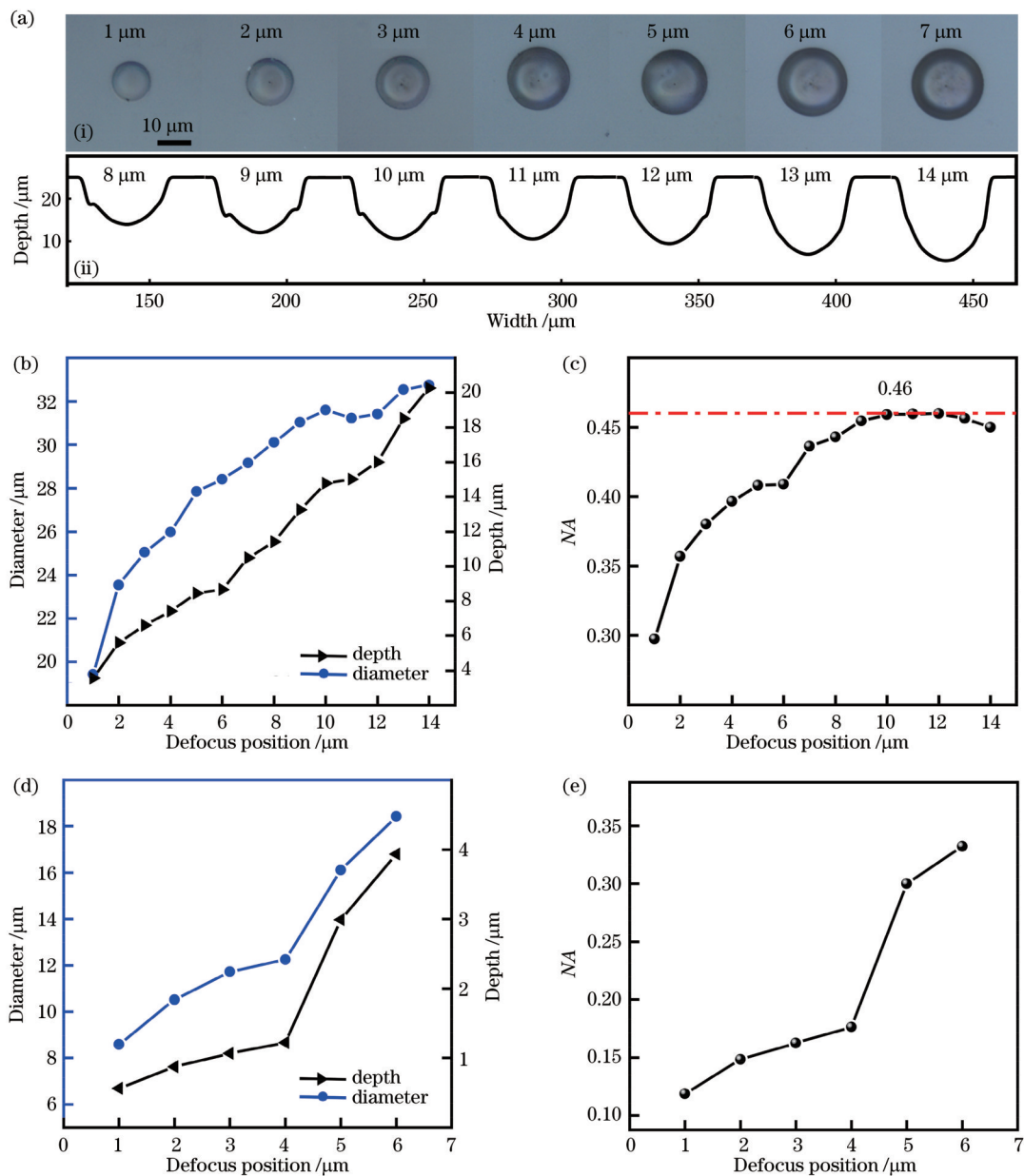


图5 自调制加工方法和常规正面加工方法在改变离焦位置时制备出的微透镜形貌参数对比。(a)自调制加工方法制备的不同离焦位置的微透镜形貌,其中(i)所示为离焦位置为1~7 μm的微透镜光学显微镜图像,(ii)所示为离焦位置为8~14 μm的微透镜共聚焦截面轮廓图;(b)自调制加工方法制备微透镜的直径和深度随离焦位置的变化;(c)自调制加工方法制备微透镜的NA随离焦位置的变化;(d)正面加工方法制备微透镜的直径和深度随离焦位置的变化;(e)正面加工方法制备微透镜的NA随离焦位置的变化

Fig. 5 Comparison of microlens morphology parameters prepared by self-modulating processing method and regular front-side processing method when changing the defocus position. (a) Morphologies of microlenses at different defocus positions using self-modulating processing method, (i) shows the optical microscope images of microlenses with defocus positions from 1 μm to 7 μm, and (ii) shows the confocal sectional profile of microlenses with defocus position from 8 μm to 14 μm; (b) diameter and depth changed with defocus position during self-modulating processing; (c) NA changed with defocus position during self-modulating processing; (d) diameter and depth changed with defocus position during front-side processing; (e) NA changed with defocus position during front-side processing

焦光斑仅在X和Y方向移动,微透镜的间隔为40 μm。激光加工后将衬底在25 °C下用20% HF溶液刻蚀90 min,得到具有高NA的大面积微透镜阵列,单个微透镜的NA为0.44,如图6所示。从图6(a)、(b)可以看到,微透镜排列整齐、大小均匀,插图中高倍显微镜

图像显示单个微透镜具有圆润的边缘以及较好的表面质量。

使用和制造大面积微透镜阵列相同的激光参数,离焦位置以1 μm为间隔从1 μm增加到9 μm,制造出一个微透镜阵列,如图7所示。该阵列由9个NA不同

表1 使用自调制法制造的微透镜的NA和其他相关论文中报道微透镜的NA

Table 1 NA for the microlens fabricated by self-modulating processing method and corresponding information reported in relevant references

Material	Method	Laser parameter	n_{silica}	NA	Ref.
Fused silica	Self-modulating	1030 nm & 300 fs	1.46	0.46	This work
Fused silica	Temporally shaped femtosecond laser	800 nm & 50 fs	1.46	0.46	[19]
Fused silica	Spatial light modulation	650 nm	1.46	0.46	[18]
Fused silica	Spatial light modulation	514 nm & 190 fs	1.46	0.41	[26]
Fused silica	Spatial light modulation	514 nm & 230 fs	1.46	0.40	[7]
Silica glass	Acousto-optic modulation	343 nm & 600 fs	1.46	0.17	[27]
K9 glass	Front-side with scanning depth	800 nm & 35 fs	1.46	0.45	[28]
Fused silica	Circularly polarized laser processing at front-side with scanning depth	800 nm & 50 fs	1.52	0.47	[29]
Silica glass	Regular front-side	800 nm & 30 fs	1.45	0.26	[30]
Glass	Regular front-side	1030 nm & 300 fs	1.46	0.23	[31]

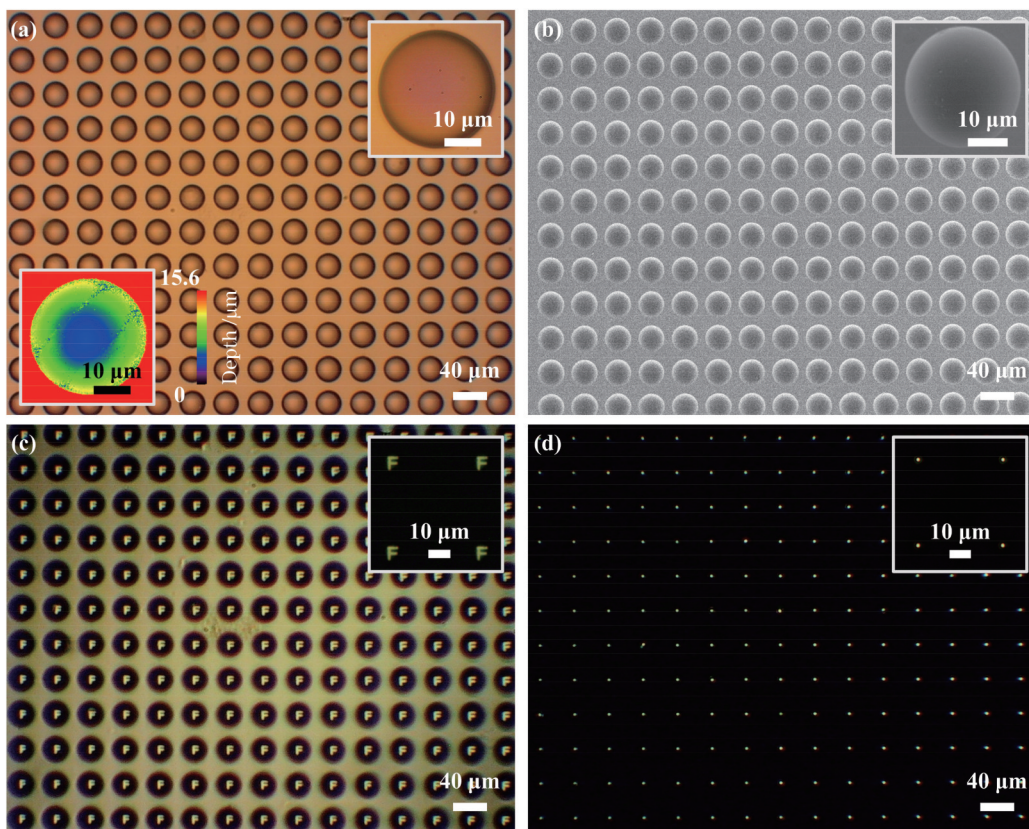


图6 大面积微透镜阵列的形貌表征和成像效果。(a)光学显微镜图像;(b)扫描电子显微镜图像;(c)光学显微镜下的成像效果;(d)光学显微镜下的聚焦效果

Fig. 6 Morphological characterization and imaging results of large-area microlens arrays. (a) Optical microscope images; (b) scanning electron microscopy images; (c) imaging results tested by optical microscopy; (d) focusing results tested by optical microscopy

的微透镜组成,每一行从左到右NA依次增加,NA的范围为0.28~0.45。

利用光学显微镜对微透镜阵列进行成像测试,并通过调整显微镜的聚焦位置,观察具有不同NA的微透镜在不同平面上的成像效果,图7(d)展示了这组微透镜的可变聚焦性能。通过调整聚焦位置,分别使第一排到第三排的微透镜达到最佳成像效果,如图7

(d1)~(d3)所示。当第一排(NA最大)的微透镜最佳成像时,第二排和第三排具有更大景深的微透镜也能较清晰地成像;当第二排(NA稍小)的微透镜最佳成像时,第一排具有小景深的微透镜成像变得更大且更模糊;当第三排(NA最小)的微透镜最佳成像时,第一排微透镜的成像已经无法分辨出字母F的形状,第二排字母F的成像相比其最佳成像时变得更大且更模

糊。这些结果验证了随着实验制造的微透镜NA增大,相应的清晰成像范围变小,证明了所制造的具有不

同NA的微透镜阵列具备在多个平面成像的能力,从而可以应用于无变焦成像等领域。

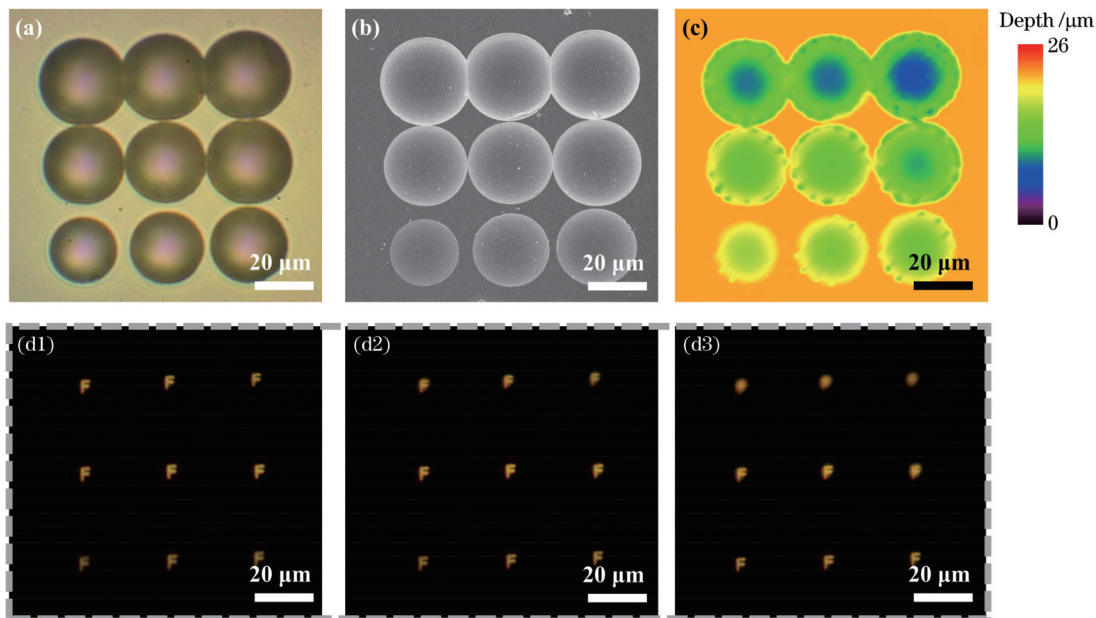


图7 具有不同NA的微透镜的形貌表征以及成像效果。(a)光学显微镜图像;(b)扫描电子显微镜图像;(c)共聚焦等高线图像;(d)成像效果,其中(d1)为第一排成像最清晰的位置,(d2)为第二排成像最清晰的位置,(d3)为第三排成像最清晰的位置

Fig. 7 Morphological characterization and imaging results of microlenses with different NA. (a) Optical microscopy image; (b) scanning electron microscopy image; (c) confocal microscopy image; (d) imaging results, (d1) clearest imaging position of the first row, (d2) clearest imaging position of the second row, and (d3) clearest imaging position of the third row

4 结 论

提出一种基于像差的自调制激光加工方法,结合HF溶液湿法刻蚀在石英背面制造出可调节数值孔径的微透镜阵列。实验结果表明,所提方法能够制造出具有NA理论最大值($NA_{max}=0.46$)的微透镜,与其他方法相比,所提方法具有步骤简单的优势,并且无需使用额外的光调制装置。此外,还探究了脉冲能量和离焦位置对于微透镜形貌和NA的影响规律。通过调节这些参数,解决了常规正面加工时改性区域深宽比小,刻蚀后微透镜NA小的问题。未来的研究可以进一步优化加工参数,提高微透镜阵列的均匀性和稳定性,以及探索其他材料和形状的微透镜阵列制造的可行性。所提方法为制造具有不同NA的微透镜阵列提供了一种新思路,在无变焦成像系统、三维成像、光束整形等领域具有巨大的应用潜力。

参 考 文 献

- [1] 郑昕,戴深宇,张玉莹,等.基于微透镜阵列的大功率紫外激光匀化技术[J].光学学报,2023,43(10): 1014005.
Zheng X, Dai S Y, Zhang Y Y, et al. UV laser homogenization technology based on microlens array[J]. Acta Optica Sinica, 2023, 43(10): 1014005.
- [2] Wang Y F, Escutie M J, Kudenov M W. Snapshot channeled imaging spectrometer using geometric phase holograms[J]. Optics Express, 2019, 27(11): 15444-15455.
- [3] Zhang Z X, Chang J, Ren H X, et al. Snapshot imaging spectrometer based on a microlens array[J]. Chinese Optics Letters, 2019, 17(1): 011101.
- [4] Liu X Q, Yang S N, Yu L, et al. Rapid engraving of artificial compound eyes from curved sapphire substrate[J]. Advanced Functional Materials, 2019, 29(18): 1900037.
- [5] Jackin B J, Jorissen L, Oi R, et al. Design and calibration of curved and see-through integral imaging 3D display[J]. Virtual Reality, 2023, 27(2): 761-775.
- [6] Wang X, Hua H. Design of a digitally switchable multifocal microlens array for integral imaging systems[J]. Optics Express, 2021, 29(21): 33771-33784.
- [7] Fan H, Cao X W, Wang L, et al. Control of diameter and numerical aperture of microlens by a single ultra-short laser pulse [J]. Optics Letters, 2019, 44(21): 5149-5152.
- [8] 李建军,褚春艳,卢玲彤,等.微透镜阵列的制备与应用研究进展[J].光学学报,2021,41(21): 2100001.
Li J J, Chu C Y, Lu W T, et al. Development of microlens arrays: from fabrication to photonic applications[J]. Acta Optica Sinica, 2021, 41(21): 2100001.
- [9] 王之岳,陈灶灶,朱利民,等.微透镜阵列单点金刚石车削补偿技术[J].光学精密工程,2022,30(7): 813-820.
Wang Z Y, Chen Z Z, Zhu L M, et al. Single point diamond turning and compensation for micro-lens array[J]. Optics and Precision Engineering, 2022, 30(7): 813-820.
- [10] 刘向阳.光刻胶热熔法制备的非球面微透镜的设计方法[J].光学学报,2019,39(2): 0208001.
Liu X Y. Design of aspheric microlens made by photoresist reflow method[J]. Acta Optica Sinica, 2019, 39(2): 0208001.
- [11] Kuang M X, Wang L B, Song Y L. Controllable printing droplets for high-resolution patterns[J]. Advanced Materials, 2014, 26(40): 6950-6958.
- [12] Roeder M, Guenther T, Zimmermann A. Review on fabrication technologies for optical mold inserts[J]. Micromachines, 2019, 10(4): 233.

- [13] Su S J, Liang J S, Li X J, et al. Direct microtip focused electrohydrodynamic jet printing of tailored microlens arrays on PDMS nanofilm-modified substrate[J]. Advanced Materials Technologies, 2021, 6(11): 2100449.
- [14] Tong S Y, Bian H, Yang Q, et al. Large-scale high quality glass microlens arrays fabricated by laser enhanced wet etching [J]. Optics Express, 2014, 22(23): 29283-29291.
- [15] Chen F, Liu H W, Yang Q, et al. Maskless fabrication of concave microlens arrays on silica glasses by a femtosecond-laser-enhanced local wet etching method[J]. Optics Express, 2010, 18(19): 20334-20343.
- [16] Liu H G, Lin W X, Hong M H. Hybrid laser precision engineering of transparent hard materials: challenges, solutions and applications[J]. Light: Science & Applications, 2021, 10: 162.
- [17] Zheng Z, Zu X T, Jiang X D, et al. Effect of HF etching on the surface quality and laser-induced damage of fused silica[J]. Optics & Laser Technology, 2012, 44(4): 1039-1042.
- [18] Liu Y, Li X W, Wang Z P, et al. Morphology adjustable microlens array fabricated by single spatially modulated femtosecond pulse[J]. Nanophotonics, 2022, 11(3): 571-581.
- [19] Qin B, Li X W, Yao Z L, et al. Fabrication of microlenses with continuously variable numerical aperture through a temporally shaped femtosecond laser[J]. Optics Express, 2021, 29(3): 4596-4606.
- [20] Sun Q A, Jiang H B, Liu Y, et al. Effect of spherical aberration on the propagation of a tightly focused femtosecond laser pulse inside fused silica[J]. Journal of Optics A, 2005, 7(11): 655-659.
- [21] Day D, Gu M. Effects of refractive-index mismatch on three-dimensional optical data-storage density in a two-photon bleaching polymer[J]. Applied Optics, 1998, 37(26): 6299-6304.
- [22] Stankevič V, Karosas J, Račiukaitis G, et al. Investigation of the modifications properties in fused silica by the deep-focused femtosecond pulses[J]. Optics Express, 2023, 31(3): 4482-4496.
- [23] 苏亚辉, 汪超炜, 韩蒙蒙, 等. 飞秒激光加工中折射率失配引起的像差问题及其矫正[J]. 光学学报, 2014, 34(s1): s122005.
- [24] Su Y H, Wang C W, Han M M, et al. Refractive-index-mismatch induced aberrations in femtosecond laser processing and its correction[J]. Acta Optica Sinica, 2014, 34(s1): s122005.
- [25] Kandidov V P, Fedorov V Y. Properties of self-focusing of elliptic beams[J]. Quantum Electronics, 2004, 34(12): 1163-1168.
- [26] Hassanin H, Mohammadkhani A, Jiang K. Fabrication of hybrid nanostructured arrays using a PDMS/PDMS replication process [J]. Lab on a Chip, 2012, 12(20): 4160-4167.
- [27] Cao X W, Chen Q D, Zhang L, et al. Single-pulse writing of a concave microlens array[J]. Optics Letters, 2018, 43(4): 831-834.
- [28] Wang Q J, Yang S R, Yang Z J, et al. Rapid fabrication of large-area concave microlens arrays on silica glasses by femtosecond laser bursts[J]. Optics Letters, 2022, 47(15): 3936-3939.
- [29] Yang T Z, Li M J, Yang Q, et al. Femtosecond laser fabrication of submillimeter microlens arrays with tunable numerical apertures[J]. Micromachines, 2022, 13(8): 1297.
- [30] Meng X W, Chen F, Yang Q, et al. A simple way to fabricate close-packed high numerical aperture microlens arrays[J]. IEEE Photonics Technology Letters, 2013, 25(14): 1336-1339.
- [31] Kotz F, Mader M, Dellen N, et al. Fused deposition modeling of microfluidic chips in polymethylmethacrylate[J]. Micromachines, 2020, 11(9): 873.
- [32] Baek G H, Hwang E S, Cheong B H. Quasi-periodic micro-lens array via laser-assisted wet etching[J]. AIP Advances, 2022, 12(10): 105219.

Fabrication of Microlens Arrays with High Numerical Aperture Based on Femtosecond Laser Self-Modulating Processing Method

Yuan Xinran¹, Deng Jingyang¹, Xu Dihua¹, Sun Xiangchao², Yu Yanhao^{2*}, Chen Qidai²

¹Guangdong Zhengye Technology Co., Ltd., Dongguan 523000, Guangdong, China;

²College of Electronic Science & Engineering, Jilin University, Changchun 130012, Jilin, China

Abstract

Objective Microlenses and microlens arrays have applications in various fields, which is primarily due to their miniaturization and easy integration. The numerical aperture (NA) is an essential parameter that significantly affects imaging quality. In the field of micro-imaging, one approach to achieve higher imaging quality is manufacturing multiple lenses with different focal lengths within a single plane. Therefore, the efficient fabrication of microlenses and microlens arrays with controllable heights is crucial for enhancing the imaging effect.

In 2010, Chen *et al.* put forward a maskless method for rapidly fabricating microlens arrays on quartz surfaces using femtosecond laser single-spot exposure combined with wet etching. This technique allows for flexible control of size and arrangement by adjusting parameters such as laser pulse energy, etching time, and displacement platform. However, one limitation of this method is that it cannot achieve deep structure due to laser energy loss caused by surface damage. As a result, the aspect ratio of the laser-modified area is small, making it challenging to fabricate microlenses with high NA.

To solve this problem, the regular front-side processing method has been improved through multiple exposures in the Z-axis direction, which increases the numerical apertures, but it cannot reach its theoretical maximum. Furthermore, researchers have conducted extensive studies on optical field modulation which have successfully produced quartz microlenses with high numerical apertures that approach the theoretical limit of 0.46. However, it should be noted that

these methods rely on precise optical devices and involve complex processes.

Methods Microlenses and their arrays are prepared by hydrofluoric acid wet-etching assisted femtosecond laser processing method, and the preparation process is divided into two steps, first using femtosecond laser to modify the material on the bottom surface, and then using 20% hydrofluoric acid for wet etching under 25 °C.

In the preparation of high aspect ratio modified regions of quartz substrates, we propose a self-modulating laser processing method based on aberrations. In this method, the femtosecond laser is focused on the lower surface of the quartz substrate, so that the closely focused laser propagates through the interface of two different materials, and the longitudinal spherical aberration caused by the mismatch of the refractive index increases the longitudinal size of the laser focusing spot. This spherical aberration phenomenon becomes more and more obvious with the increase of the numerical aperture of the objective lens and the depth of focus, which enables the longitudinal stretching of the laser focus, resulting in the processing of modified areas with high aspect ratios on the quartz substrate.

Microlenses and microlens arrays have been prepared by laser with a pulse width of about 300 fs and a wavelength of 1030 nm combined with a three-dimensional air flotation platform. Firstly, the influence of pulse energy on the morphology and numerical aperture of microlenses has been explored by the control variable method. On this basis, the defocus position has been regulated, which effectively increases the numerical aperture of the microlens, and a high numerical aperture quartz microlens that reached the theoretical limit has been successfully prepared.

Results and Discussions First, the same parameters are used to compare the process of microlens formation during wet etching in regular front-side processing and self-modulating processing, which proves the advantages of self-modulating processing in the modified region with a high aspect ratio (Fig. 3).

Next, the morphological characteristics of microlenses processed under different laser single pulse energies using the self-modulating method are explored. With the increase of laser single pulse energy, the change of the radius of curvature is 1.46 μm, the change range of NA is 0.19–0.41, and the NA reaches 0.41 (Fig. 4) when the single pulse energy is 309 nJ. On this basis, the defocus position is changed, and the lens parameters processed by regular front-side processing and self-modulating method are compared. The depth and width of the microlenses prepared by the two processing methods increase approximately linearly with the increase of the defocus position, and the width of the microlenses processed by the self-modulating method is slightly larger than that of the microlenses prepared by the front-side processing method, and its depth is close to twice that of the front-side processed microlenses. The maximum value of the lens prepared by the front-side method is only 0.33, while the theoretical limit value of the lens (0.46) is reached by the self-modulating method at the defocus position of 11 μm (Fig. 5).

Finally, a large-area microlens array with $NA=0.44$ has been prepared on the back of the quartz substrate by laser self-modulating method. The microlenses are neatly arranged, uniformly sized, with rounded edges and good surface quality (Fig. 6). Furthermore, by changing the defocus position, a microlens array composed of 9 microlenses with different NA has been prepared, and the NA range is 0.28–0.45 (Fig. 7). These two structures prove the feasibility of laser self-modulating method in processing large-area microlens arrays with tunable NA.

Conclusions We propose a novel method for fabricating microlens arrays on the back side of quartz by an aberration-based self-modulating laser processing technique, and this method allows for producing microlenses with adjustable numerical apertures to achieve the theoretical maximum value ($NA_{max}=0.46$). The essential advantage of this approach is its simplicity compared with other methods, as it does not require additional optical modulation devices. Experimental results demonstrate the successful fabrication of microlenses using this method. Furthermore, our study investigates the effects of pulse energy and defocus position on the shape and numerical aperture of the microlenses. By adjusting these parameters, the problem of a small aspect ratio in the modified region during regular front-side processing is effectively resolved.

Future research can focus on optimizing the processing parameters to enhance the uniformity and stability of the fabricated microlens arrays. Additionally, exploring the feasibility of fabricating microlens arrays through different materials and shapes would be a helpful direction for further investigation. Overall, we present an effective method for fabricating microlens arrays with various shapes. This technique has great potential for applications in zoom-free imaging systems, 3D imaging, and beam shaping.

Key words laser technique; femtosecond laser processing; high numerical aperture; microlens arrays; fused silica